High-Frequency 94 GHz ENDOR Characterization of the Metal Binding Site in Wild-Type Ras·GDP and Its Oncogenic Mutant G12V in Frozen Solution†

M. Bennati,*,‡ M. M. Hertel,‡ J. Fritscher,‡ T. F. Prisner,‡ N. Weiden,# R. Hofweber,§ M. Spörner,§ G. Horn,§ and H. R. Kalbitzer§

Institute of Physical and Theoretical Chemistry and Center for Biomolecular Magnetic Resonance, J. W. Goethe University of Frankfurt, D-60439 Frankfurt, Germany, Institute of Physical Chemistry III, Darmstadt University of Technology, D-64287 Darmstadt, Germany, and Institute of Biophysics and Physical Biochemistry, University of Regensburg, 93053 Regensburg, Germany

Received June 15, 2005; Revised Manuscript Received September 22, 2005

ABSTRACT: The guanine nucleotide binding protein Ras plays a central role as molecular switch in cellular signal transduction. Ras cycles between a GDP-bound "off" state and a GTP-bound "on" state. Specific oncogenic mutations in the Ras protein are found in up to 30% of all human tumors. Previous ^{31}P NMR studies had demonstrated that in liquid solution different conformational states in the GDP-bound as well as in the GTP-bound form coexist. High-field EPR spectroscopy of the GDP complexes in solution displayed differences in the ligand sphere of the wild-type complex as compared to its oncogenic mutant Ras-(G12V). Only three water ligands were found in the former with respect to four in the G12V mutant [Rohrer, M. et al. (2001) *Biochemistry 40*, 1884−1889]. These differences were not detected in previous X-ray structures in the crystalline state. In this paper, we employ high-frequency electron nuclear double resonance (ENDOR) spectroscopy to probe the ligand sphere of the metal ion in the GDP-bound state. This technique in combination with selective isotope labeling has enabled us to detect the resonances of nuclei in the first ligand sphere of the ion with high spectral resolution. We have observed the ^{17}O ENDOR spectra of the water ligands, and we have accurately determined the ^{17}O hyperfine coupling with $a_{iso} = -0.276$ mT, supporting the results of previous line shape analysis in solution. Further, the distinct resonances of the α-, β-, and γ-phosphorus of the bound nucleotides are illustrated in the ^{31}P ENDOR spectra, and their hyperfine tensors lead to distances in agreement with the X-ray structures. Finally, ^{13}C ENDOR spectra of uniformly ^{13}C-labeled Ras(wt)·GDP and Ras(G12V)·GDP complexes as well as of the Ras-(wt)·GppNHp and the selectively 1,4-^{13}C-Asp labeled Ras(wt)·GDP complexes have revealed that in frozen solution only one amino acid is ligated to the ion in the GDP state, whereas two are bound in the GppNHp complex. Our results suggest that a second conformational state of the protein, if correlated with a different ligand sphere of the Mn^{2+} ion, is not populated in the GDP form of Ras at low temperatures in frozen solution.

The human Ras (rat sarcoma) protein plays a central role as molecular switch in cellular signal transduction, regulating important processes such as differentiation, proliferation, and apoptosis of cells (see, for example, ref *1*). Specific oncogenic mutations in Ras proteins can be found in up to 30% of all human tumors (*2*). Ras (and the other members of the Ras superfamily) bind Mg^{2+}·GDP[1] and Mg^{2+}·GTP with nanomolar to picomolar affinity in the active center if an excess of Mg^{2+} is present. With GTP bound, Ras interacts with effectors such as Raf-kinase or PI(3)-kinase and activates the corresponding signaling pathway. Activation is performed by guanine nucleotide exchange factors (GEFs), such as Sos (from the *Drosophila* gene *son-of-sevenless*), which catalyze the exchange of GDP against GTP. The signal is switched off when GTP is hydrolyzed to GDP either by the intrinsic GTPase activity of Ras or by GTPase activating proteins (GAPs). The oncogenic variants contain point mutations, which block the GTPase activity in the presence and absence of GAP. This leads to the accumulation of Ras in the active form and thus contributes to tumor formation. Since the bound nucleotides control the activation state of the protein, a detailed knowledge of their interaction with the surroundings is of central importance.

Several X-ray structures of Ras alone or in complex with GEFs, GAPs, and effectors have been published that give a detailed view of the nucleotide binding in the GDP and GTP form in the wild-type (wt) protein as well as in oncogenic mutants. The active site contains the important divalent ion

† This work was supported by the DFG high priority program 1051.

* Corresponding author. Phone: +49 69 798 29 590. Fax: +49 69 798 29 404. E-mail: bennati@chemie.uni-frankfurt.de.

‡ J. W. Goethe University of Frankfurt.

Darmstadt University of Technology.

§ University of Regensburg.

[1] Abbreviations: DSS, 2,2-dimethyl-2-silapentane-5-sulfonate; DTE, 1,4-dithioerythritol; G12V, mutation of glycine 12 to valine; GDP, guanosine-5′-diphosphate; GEF, guanine nucleotide exchange factor; GppNHp, guanosine-5′-(β,γ-imido)triphosphate; GTP, guanosine-5′-triphosphate; hfc, hyperfine coupling; HEPES, 4-(2-hydroxyethyl)-1-piperazineethanesulfonic acid; PI(3), phosphinositol(3); Raf, rapid fibrosarcoma; RBD, ras binding domain; RhoA, product of the rhoA gene; Tris, Tris(hydroxymethyl)amimnomethane.

10.1021/bi051156k CCC: $33.50
Published on Web 12/08/2005

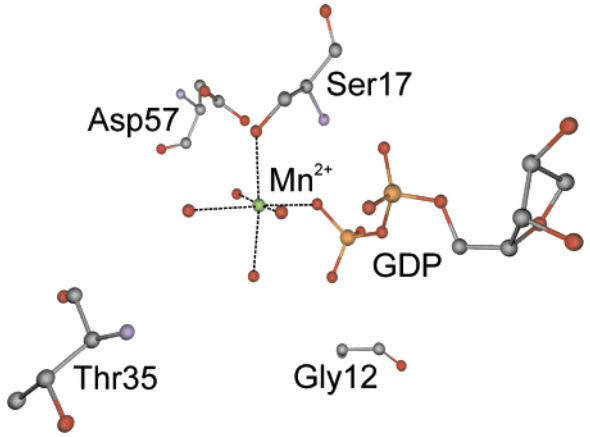

FIGURE 1: Structure of the metal−GDP complex of Ras. The coordination of Mn^{2+}·GDP in Ras is depicted from the X-ray structure of ref *4*. The structure shows Ser17 as the only amino acid ligated to the metal and the oxygen of the β-phosphate group of GDP as the only ligand from the nucleotide. The four other ligands are water molecules.

Mg^{2+} as cofactor in both the GDP- and the GTP-bound forms (*3*, *4*). The phosphate groups of GDP and GTP interact with the functional groups of the protein as well as with the Mg^{2+} ion and with several water molecules. The arrangement of the active site with the coordination scheme of the metal−nucleotide complex in the GDP-bound form is depicted from the crystal structure of Tong et al. (*4*) in Figure 1.

The Mg^{2+} ion is coordinated to an oxygen of the β-phosphate group of GDP, to the oxygen of the hydroxyl group of Ser17, and to four water molecules. Three of the water molecules are arranged in an equatorial position, and one is positioned axially within the octahedral configuration around the central metal ion. In one of the published X-ray structures (*3*), differences between the GDP and GTP bound states are reported in a region around Asp57. According to this study, Asp57 is directly coordinated to the metal ion in the GDP-bound form but via an intervening water molecule in the GTP-bound form. Three water ligands are also found in the X-ray structures from the Mg^{2+}·GDP complex of the human small GTPase RhoA (*5*), where the main chain carbonyl of Thr35 is directly coordinated to the metal ion.

Two coordinating water molecules are replaced in the GTP-bound form by an oxygen of the γ-phosphate group and an oxygen of the hydroxyl group of Thr35, a residue strictly conserved in the members of the Ras superfamily. A couple of Ras mutants were also structurally investigated, most notably the oncogenic mutants G12V, G12R, G12D, and Q61L (*6*−*8*). They showed a similar overall structure as the wild-type protein.

Liquid-state nuclear magnetic resonance (NMR) (*9*−*13*), Fourier transform infrared (FTIR) (*14*−*16*), Raman (*17*) and molecular dynamics (MD) (*18*−*20*) studies gave evidence for the important role of structural dynamics and suggest the existence of more than one conformational state in Ras. Particularly, different conformational states were found by ^{31}P NMR for the GDP (*21*) and GTP complexes (*11*, *13*, *22*, *23*). These dynamic equilibria can be perturbed by minor changes in the amino acid sequence or the type of nucleotide analogue bound to Ras. According to these studies, the Ras(wt)·GDP complex occurs in two conformational states 1 and 2 with an equilibrium constant K_{12} of 0.31, whereas the oncogenic mutant Ras(G12V) occurs predominantly in state 1 ($K_{12} < 0.04$) (*21*).

To obtain more details about the structure of the active site in solution, electron paramagnetic resonance (EPR) spectroscopy has been applied by several groups after substitution of the diamagnetic magnesium ion with a paramagnetic manganese ion (*21*, *24*, *25*). A crystal structure of a Ras(G12P)·CppCp complex containing a manganese ion showed a very similar ligand sphere as the same complex containing a magnesium ion (*26*). After normal water was exchanged with ^{17}O-enriched water, the hyperfine interaction between the metal ion and the ^{17}O nuclei of the water molecules becomes visible and allows one to extract the number of coordinated water molecules at high magnetic field values. In the GDP-bound form of the G12V mutant, all EPR studies gave consistently the same number of four water molecules bound to the metal center as revealed by the crystal structure (*6*). These results were also supported by electron spin−echo envelope modulation (ESEEM) studies (*27*−*29*), which determined distances between the Mn^{2+} and selectively isotope-labeled nuclei very similar to those calculated from the crystal structures. In contrast, high-field EPR (HF-EPR) measurements on the wild-type sample at room temperature showed only three water molecules in the ligand sphere of the manganese ion in the GDP complex (*21*). For the first time, spectroscopic results showed a difference in the ligand sphere of the catalytic center between the wild-type and the oncogenic mutant of the protein−nucleotide complex in its inactive state. HF-EPR measurements on the wild-type sample at low temperature exhibited additional line broadening and did not allow to extract the number of coordinated water molecules (*25*). The question about the nature of the ligand that would replace one water molecule in the Ras(wt)·GDP complex is the starting point of the present investigation.

In the past few years, electron nuclear double resonance (ENDOR) at high microwave frequencies (HF-ENDOR) has been established as a powerful technique to detect the resonances of nuclei close to a paramagnetic center in proteins (*30*, *31*). This technique is uniquely suited to observe structural details of the ligand assembly to a paramagnetic center within the protein in frozen solution. In contrast to the standard ENDOR and ESEEM techniques at X-band (9 GHz), HF-ENDOR has a much better spectral resolution for low-gamma nuclei and hyperfine line shapes become easy to analyze because the high-field conditions suppress second-order effects in the hyperfine interaction.

In the present study, we employ HF-ENDOR in combination with selective isotope labeling to detect the resonances of ^{17}O, ^{31}P, and ^{13}C nuclei in the first ligand sphere of the Mn^{2+} ion in the Ras·Mn^{2+}·GDP complex and to search for the ligand that was proposed to replace the water molecule in the wild-type GDP complex in solution. We propose that two types of ligands are the most likely candidates, either a phosphate ion or a second amino acid from the protein active site. We compare the spectrum of the wild-type Ras·GDP complex with that obtained from its oncogenic mutant Ras(G12V) and with spectra of the non-hydrolyzable GTP analogue GppNHp (used as a reference).

MATERIALS AND METHODS

Protein Purification. Wild-type human H-Ras (aa 1−189) and its mutant Ras(G12V) were expressed in *Escherichia coli* and purified as described before (*32*). $^{15}N/^{13}C$-labeled proteins were expressed in $^{15}N/^{13}C$-enriched medium (Silantes, Munich). Final purity of the protein was >95% as judged from the sodium dodecyl sulfate−polyacrylamide gel electrophoresis. By reversed phase HPLC, the complete loading of the proteins with GDP was controlled. Nucleotide exchange to GppNHp was done using alkaline phosphatase treatment in the presence of a 2-fold excess of the GTP analogue as described at John et al. (*33*). The Ras-binding domain of human cRaf-1 (Raf-RBD, amino acids 51−131) was expressed in *E. coli* and purified as described before (*34*).

Synthesis of ^{13}C-Aspartate Labeled Samples. ^{13}C-labeled Ras(wt) was synthesized by *E. coli* based cell-free protein expression. The continuous exchange cell free reaction was carried out in a DispoDialyzer (SpectraPor, MWCO 50 000 Da) according to ref *35*. The reaction solution (1 mL) consisted of 0.65 mM 3′,5′-cyclo AMP, 0.1 mM of each of the 20 amino acids (aspartate was 1,4-^{13}C-labeled), 27.64 mM ammonium acetate, 1.22 mM ATP, 0.25 mg/mL creatine kinase, 80.85 mM creatine phosphate, 0.87 mM of CTP, GTP, and UTP, 1.77 mM DTT, 36% (v/v) *E. coli* S-30 extract, 0.168 mg/mL *E. coli* tRNA (MRE 600), 57.96 mM HEPES−KOH (pH 7.5), 201.98 mM potassium glutamate, 0.034 mg/mL L-(−)-5-formyl-5,6,7,8-tetrahydrofolic acid, 4 mM magnesium acetate, 4.028% (w/v) PEG 8000, 0.02 mg/mL plasmid-DNA (pK7ras), protease inhibitor 1×, 560 U/mL RNase-inhibitor and 0.045 mg/mL T7 RNA polymerase. The volume was 30 μL, and the reaction was performed for 1 h by shaking at 37 °C. The external feeding solution (10 mL) consisted of 0.65 mM 3′,5′-cyclo AMP, 0.1 mM of each of the 20 amino acids (aspartate was 1,4 ^{13}C-labeled), 27.64 mM ammonium acetate, 1.22 mM ATP, 0.25 mg/mL creatine kinase, 80.85 mM creatine phosphate, 0.87 mM of CTP, GTP, and UTP, 1.77 mM DTT, 0.168 mg/mL *E. coli* tRNA (MRE 600), 57.96 mM HEPES−KOH (pH 7.5), 201.98 mM potassium glutamate, 0.034 mg/mL L-(−)-5-formyl-5,6,7,8-tetrahydrofolic acid, 4 mM magnesium acetate, 4.028% (w/v) PEG 8000. The reaction was carried out for 20 h at 37 °C at 260 rpm. After 10 h, the feeding solution was changed and plasmid, T7 RNA polymerase and creatine kinase were supplemented. The T7 RNA polymerase was prepared according to ref *36*. The *E. coli* S30 cell extract was prepared according to ref *37* with various modifications. The *E. coli* strain used was BL21DE3; the cultures were grown to a $OD_{595\ nm}$ of 1 and then rapidly cooled to 4 °C. The cell disruption was done by sonification. The final extract was condensed by PEG 8000 preciptiation followed by ultrafiltration in a Vivaspin 20 (MWCO 3000). The purification of Ras was carried out according to ref *38*.

Preparation of Mn^{2+} Samples. Ras·Mn^{2+}·GDP or Ras·Mn^{2+}·GppNHp was prepared by incubation of 100 μM Ras·Mg^{2+}·GDP in 50 mM Tris-HCl, pH 7.6, 5 mM DTE, 300 mM $(NH_4)_2SO_4$, and 200 mM $MnCl_2$ overnight at 278 K. Salts and excess $MnCl_2$ were separated by gel filtration in 40 mM HEPES−NaOH, pH 7.4, and 2 mM DTE. Samples with $H_2{}^{17}O$ were obtained by lyophilizing frozen samples and dissolving the protein in the same amount of $H_2{}^{17}O$ (46.3%, Isotec). About 5 μL of the sample were loaded in quartz capillary tubes for W-band (0.9 OD), shock frozen in liquid nitrogen, and inserted into the precooled cryostat at about 100 K.

Pulsed ENDOR Spectroscopy. All experiments were performed on a Bruker E680 W-band (94 GHz) spectrometer equipped with a homemade ENDOR probe head and a 94 GHz microwave amplifier (about 20 dBm output) from Donetsk Physico Technical Institute. Davies ENDOR spectra were typically acquired with a pulse sequence (π−RF−π/2−π) consisting of selective pulses, with typical $\pi/2$ pulse lengths 50−100 ns for $S = 5/2$ of the Mn^{2+}. The sequence was employed to detect couplings larger than approximately 4−5 MHz as to be expected in the ^{17}O or ^{31}P spectra. Mims ENDOR ($\pi/2-\tau-\pi/2-$RF$-\pi/2$) was used to detect weak hyperfine couplings as encountered in the ^{13}C spectra. The length of the radio frequency (RF) pulse varied for the different nuclei and was optimized for a maximum ENDOR effect. All experiments were performed at temperatures between 3 and 4 K with a shot repetition time between 15 and 25 ms. More detailed parameters are given for each experiment in the figure captions.

ENDOR Simulations. Simulations were performed using home-written MATLAB routines described previously (*39*). For simplicity, the simulations were performed only for the ENDOR lines arising from the EPR $m_S = +1/2$ to $-1/2$ transition of the $S = 5/2$ Mn^{2+} spin, where m_S is the electron spin quantum number. At high fields, these ENDOR lines are well resolved and expected at the first-order frequencies:

$$\nu_{\pm}(m_I) = |\nu_{0I} \pm m_S A^I_{zz} + 3 \cdot Q^I_{zz}(2 \cdot m_I - 1)|$$

where ν_{0I} is the nuclear Zeeman frequency of nucleus I, m_I the nuclear spin quantum number, A_{zz} and Q_{zz} are the orientation-dependent hyperfine and quadrupole tensor components and m_S can have values ±1/2, ±3/2, and ±5/2. The high-field approximation is generally valid when the nuclear Zeeman frequencies are substantially larger than the observed hyperfine couplings, which is here the case for ^{31}P ($\nu_{0I} =$ 57.4 MHz) and ^{13}C ($\nu_{0I} = 36.2$ MHz). For ^{17}O ($\nu_{0I} = 19.5$ MHz), one might take into account the Hamiltonian up to pseudo first order, i.e. the I_x and I_y nuclear spin components should be considered. However, we found that the hyperfine interaction observed is mostly isotropic and leads to negligible contributions of the nondiagonal terms A_{xz} and A_{yz}.

The zero-field splitting (ZFS) term of the electron spin Hamiltonian for the Ras·Mn^{2+}·GDP complex is small ($D \approx$ 11 mT, $E \approx 0$) and contributes to the $\Delta m_S = +1/2$ to $-1/2$ transition only as second-order perturbation (*21*). Further, *g*-anisotropy and the anisotropy of the ^{55}Mn hyperfine coupling can be neglected (*21*). Thus, orientational selectivity has not to be taken into account to compute the ENDOR transitions associated to the electron $m_S = \pm 1/2$ manifolds. The validity of this assumption is demonstrated by the satisfactory agreement between the computed and the experimental ENDOR line shapes.

RESULTS AND DISCUSSION

^{17}O ENDOR Spectra. We started our comparative investigation on the wild-type Ras·Mn^{2+}·GDP complex and its oncogenic mutant Ras(G12V) by recording the ^{17}O ENDOR

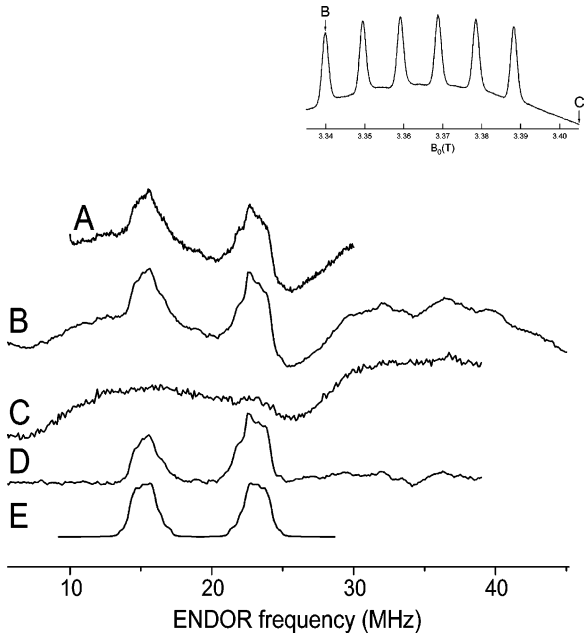

FIGURE 2: ^{17}O Davies ENDOR spectra of Ras(G12V)·Mn^{2+}·GDP (A) and Ras(wt)·Mn^{2+}·GDP (B) measured on the central $m_s = +1/2$ to $-1/2$ transition (first Mn hyperfine line) (see inset). Spectrum C is recorded at a spectral position, where only the higher m_s transitions contribute. Subtraction of spectrum C from spectrum B leads to spectrum D, which shows the contribution of the central $m_s = +1/2$ to $-1/2$ transition. (E) Simulation of spectrum D with the parameters given in the text. Experimental parameters: MW inversion pulse $t_\pi = 180$ ns, $t_{\pi/2} = 100$ ns, $\tau = 250$ ns, $t_{RF} = 22$ μs, 10 shots per point. Number of scans: (A) 45; (B) 15; (C) 20.

spectra of the water molecules coordinated to the Mn^{2+} ion. All previous continuous wave (CW) EPR studies performed to count the number of the coordinated water molecules in these complexes (*21*) had been based on the analysis of the hyperfine broadening produced by the H_2O-^{17}O nuclei on the Mn^{2+} EPR lines; however, the precise value of the ^{17}O hyperfine coupling (hfc) has been unknown. HF-ENDOR spectroscopy represents the most direct method to measure this hfc. This has also been demonstrated in recent HF-ENDOR work on Gd^{3+} aqua ion in $H_2{}^{17}O$ (*40*). The ^{17}O Davies ENDOR spectra of the Ras·GDP complexes are illustrated in Figure 2.

To eliminate baseline distortions and to separate the central transition ($m_S = +1/2$ to $-1/2$) from contributions of the other electron spin transitions, we recorded a reference ENDOR spectrum (Figure 2C) excited outside the range of the electron $m_S = \pm 1/2$ transition. Subtraction of spectrum C from B (Figure 2D) clearly indicates a structured doublet centered at the expected ^{17}O nuclear Zeeman frequency (19.5 MHz) and split by ≈ 8 MHz, which we assign to the ENDOR lines arising from the EPR $m_S = \pm 1/2$ manifolds. The shape of the doublet powder pattern is generated by the concomitant effect of the anisotropic hyperfine interaction and the quadrupole interaction with the ^{17}O I = 5/2 nucleus. To analyze the pattern, we performed simulations of the spectrum of Ras(wt)·Mn^{2+}·GDP (Figure 2D) and obtained satisfactory agreement with the experiment for one set of tensor parameters: $|A_x| = 6.27$ MHz, $|A_y| = 6.86$ MHz, $|A_z| = 10.10$ MHz, $Q_x = -0.238$ MHz, $Q_y = 0.238$ MHz, $Q_z = 0$ and the Euler angles $\alpha = 15°$, $\beta = 35°$, $\gamma = 0°$ (Table 1). Here the Euler angles represent the mutual orientation of the hyperfine and the quadrupole tensor. Additional simulations with slightly varied hfc and quadrupole tensor parameters (data not shown) indicated that the accuracy in the determination of the quadrupole tensor parameters is about 10%, whereas it is higher (less than 10%) for a_{iso}.

The hfc and quadrupole tensor components are very similar to the ones previously reported by Tan et al. (*41*) for a Mn^{2+} aqua complex ($A_\perp = -6.5$ MHz, $A_{||} = -9.5$ MHz and $-Q_x = Q_y = 0.35$ MHz, $Q_z = 0.0$ MHz), which were determined using a much more complex spectroscopic approach of combined ESEEM, ENDOR as well as CW techniques at X-band frequencies.[2] Our results indicate that all ^{17}O nuclei of the coordinated water molecules are magnetically equivalent within the ENDOR line width; therefore, it is not possible to count the number of water molecules from the observed spectrum. Furthermore, the ^{17}O ENDOR spectrum of the G12V mutant does not show any significant difference with respect to the spectrum of the wild-type protein.

From the shape of the ENDOR lines, we deduce that all three hyperfine tensor components have the same sign, and this sign can be determined in the high-field ENDOR experiment from the asymmetry of the lines in conjunction with a measurement of the ENDOR spectrum outside of the $-1/2 \rightarrow +1/2$ transition (*42*). In a high-spin system with weak ZFS such as Mn^{2+}, asymmetry effects in ENDOR occur by excitation of either transition associated with the higher electron spin manifolds $\pm 3/2$ and $\pm 5/2$ since negative manifolds are more largely populated than the positive ones. These higher transitions are partially excited simultaneously with the $m_S = \pm 1/2$ transition. For a nuclear spin system with a negative γ value such as ^{17}O, it is expected that the ENDOR line associated with the electronic $-3/2 \rightarrow -1/2$ transition appears at the low-frequency side for a positive hfc or vice versa for a negative hfc. Since our spectrum displays a larger amplitude at the high-frequency site and spectrum C recorded far outside the range of the $-1/2 \rightarrow +1/2$ transition consistently displays a weak contribution of the peak around 22 MHz (from the $-3/2 \rightarrow -1/2$ transition), the ^{17}O hfc must be negative in accordance with previous reports (*41*).

From the principal values of the ^{17}O hyperfine tensor, we are now able to extract the isotropic hfc, which results in -7.74 MHz or -0.276 mT (Table 1). In the previous HF-EPR studies at room temperature for a number of mutants (*21*), the simulated ^{17}O hfc values spread between |0.25| and |0.28| mT. However, for the wild-type protein a best value of |0.274| mT was found in combination with a fit of the ^{17}O broadening with three water molecules. The agreement between the previously simulated and the experimental ^{17}O hfc provides new support for the results of the previous EPR analysis.

^{31}P ENDOR Spectra. In principle, after the hydrolysis of GTP by Ras, a transient GDP·P_i complex is formed in which the inorganic phosphate P_i is noncovalently bound to the protein. Under equilibrium conditions, such a complex is always formed when P_i is present in solution, and its population is defined by the free P_i concentration and the corresponding association constant. Although the Ras prepa-

[2] During the process of revision of this paper, another HF-ENDOR study on the Mn^{2+} aqua complex [Baute D., and Goldfarb, D. (2005) *J. Phys. Chem. A 109*, 7865−7871] appeared that reported very similar hfc and quadrupole parameters as found in the present study.

Table 1: Hyperfine Tensor Components Obtained from ENDOR Studies[a]

nucleus	nucleotide	A_1	A_2	A_3	a_{iso}	$T_\perp$	R_{exp} [Å]	R_{lit} [Å]
^{17}O	GDP	−6.2	−6.8	−10.1	−7.7			
$^{31}P_\alpha$	GDP	0.28	0.28	0.62	0.02	0.26	4.9	4.59 (*4*)
								4.45 (*44*)
								4.66 (*45*)
								5.3 (*27*)
$^{31}P_\beta$	GDP	3.90	3.90	6.40	4.70	−0.80	3.4	3.46 (*4*)
								3.16 (*44*)
								3.50 (*45*)
								3.3 (*27*)
$^{31}P_\gamma$	GppNHp	3.30	3.30	5.80	4.13	−0.83	3.4	3.25 (*47*)
								3.24 (*48*)
^{13}C (Ser17)	GDP	−0.19	−0.19	+1.76	+0.46	−0.65	3.1	3.49 (*4*)
		(+0.07)	(+0.19)	(+1.63)	(+0.62)	(−0.49)		3.45 (*44*)
								3.25 (*45*)
^{13}C (Thr35)	GppNHp	−0.07	−0.07	+1.72	+0.62	−0.55	3.3	3.16 (*47*)
		(−0.03)	(+0.13)	(+1.91)	(+0.67)	(−0.63)		3.15 (*48*)
^{13}C (Ser17)	GppNHp	+0.52	+0.52	+2.02	+1.02	−0.50	3.4	3.24 (*47*)
		(+0.27)	(+0.42)	(2.10)	(+0.93)	(−0.59)		3.31 (*48*)

[a] All hyperfine values are given in MHz. In parentheses are the values from DFT calculations (see Appendix). For ^{13}C couplings, the sign of the largest tensor component was taken from the DFT calculations. For the ^{31}P couplings, the tensor components have all the same sign, which is either positive or negative.

ration was performed with phosphate-free buffers and no free P_i or bound P_i can be detected by ^{31}P NMR spectroscopy in solutions of Ras·GDP, we cannot exclude that in GDP-bound form a further noncovalently bound phosphate exists as contamination from the cell-lysate in the active site of Ras. It could replace a water molecule, and an additional ^{31}P resonance should be observed in the ENDOR spectra. Furthermore, our previous NMR experiments in liquid solution (*21*) had given evidence for some dynamics in the structural environment of the β-phosphate group of the bound GDP nucleotide; in particular, two conformational states were detected in the wild-type protein, whereas only one was found in the G12V. Two conformational states around the β-phosphate group of the Ras(wt)·GDP complex were also postulated from the FTIR spectra of the phosphate vibrations (*16*). These results have prompted us to examine the ^{31}P ENDOR spectra of the two Ras variants.

The ^{31}P Davies ENDOR spectra of the wild-type protein and the G12V mutant are displayed in Figure 3A,B and show a symmetric doublet centered at the ^{31}P Larmor frequency of 57.4 MHz. The shape of each line is typical for an anisotropic hyperfine tensor, and the splitting of the doublet is given by the isotropic hyperfine coupling a_{iso}. To search for additional resonances, we have also recorded Mims ENDOR spectra, as illustrated in Figure 3C,D. The spectra clearly show another doublet with a much smaller splitting. Considering the structure of the Mn^{2+}·GDP complex depicted in Figure 1, we have assigned the doublet with the larger hyperfine couplings to the β-phosphorus and the second to the α-phosphorus of the bound GDP. We note that the spectra of both compounds, the wild-type and the G12V mutant, show a very similar line shape within the signal-to-noise, with the maxima and the width of the powder pattern at the same spectral positions as marked in Figure 3. The Davies and Mims ENDOR spectra were simulated with the tensor parameters: $|A_{\perp 1}| = 4.09$ MHz, $|A_{||1}| = 6.72$ MHz and $|A_{\perp 2}| = 0.28$ MHz, $|A_{||2}| = 0.56$ MHz, respectively, using the same parameters for both compounds. This result indicates that we cannot establish differences from the ^{31}P ENDOR spectra

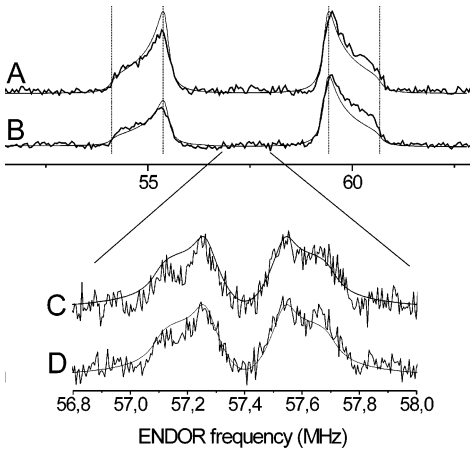

FIGURE 3: ^{31}P Davies (A, B) and Mims (C, D) ENDOR spectra of Ras(wt)·Mn^{2+}·GDP (upper traces) and of Ras(G12V)·Mn^{2+}·GDP (lower traces) measured at 4 K. Experimental parameters: MW inversion pulse $t_\pi = 200$ ns, $t_{\pi/2} = 110$ ns, τ (Mims) = 400 ns, $t_{RF} = 15$ μs, 20 shots per point. Number of scans: (A) 13; (B) 25; (C) 13; (D) 36. Dotted lines: simulations with parameters as given in the text. In spectrum B, the intensity of the simulation was normalized separately for the two halves of the spectrum for a better comparison with the experimental results.

of the wild-type and the G12V mutant within the line width. This result is not necessarily in contradiction with the finding of two conformational states by ^{31}P NMR spectroscopy since ENDOR spectra are dominated by the hyperfine interaction with the paramagnetic ion, whereas the NMR spectra are recorded in the diamagnetic state and therefore chemical shifts are more sensitive to the local structural and chemical environment of the nuclei. Furthermore, as an important difference, the NMR and also the FTIR data were recorded in liquid solution, whereas the present data are in the frozen state at low temperatures.

The traceless dipolar part of the hfc tensors can be used to estimate the distance between the Mn^{2+} ion and the ^{31}P nuclei in a simple point-dipole model:

$$T_\perp = \frac{g_e \cdot g_n \cdot \beta_e \cdot \beta_n}{h \cdot r^3}$$

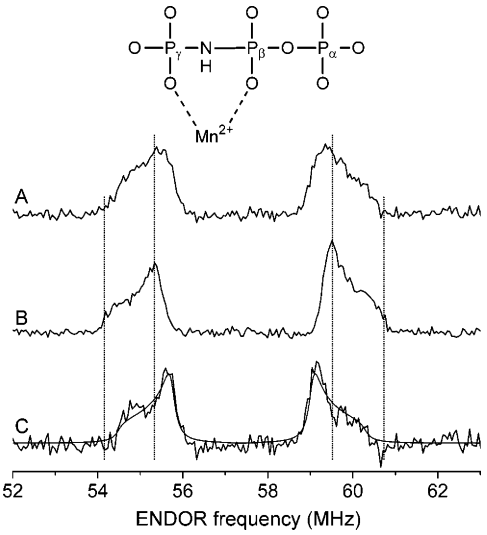

FIGURE 4: Comparison of the ^{31}P Davies ENDOR spectra of Ras(wt)·Mn^{2+}·GppNHp (A) and of Ras(wt)·Mn^{2+}·GDP (B). Subtraction of B, normalized to 50% of the area of A, from A results in C. Superimposed to C is a simulation with the parameters given in the text. Inset: Schematic structure of the ligand arrangement around the metal ion in the complex with the GppNHp. Experimental parameters: $t_\pi = 160$ ns, $t_{RF} = 16$ μs, $t_{\pi/2} = 90$ ns, $\tau = 400$ ns, 50 scans with 20 shots per point. (B) as in Figure 3A.

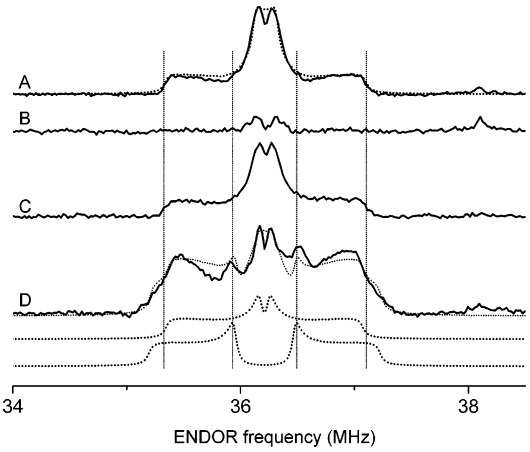

FIGURE 5: ^{13}C Mims ENDOR spectra of uniformly ^{13}C-labeled Ras(wt)·Mn^{2+}·GDP (A), of selectively ^{13}C-1,4 Asp57 labeled Ras(wt)·Mn^{2+}·GDP (B), of uniformly ^{13}C-labeled Ras(G12V)·Mn^{2+}·GDP (C) and of uniformly ^{13}C-labeled Ras(wt)·Mn^{2+}·GppNHp·Raf-RBD (D). Experimental parameters: (A) $t_{\pi/2} = 96$ ns, $\tau = 250$ ns, $t_{RF} = 18$ μs, 240 scans, 50 shots per point (B) $t_{\pi/2} = 32$ ns, $\tau = 500$ ns, $t_{RF} = 46$ μs, 202 scans, 20 shots per point. (C) as (A) but with $t_{\pi/2} = 42$ ns. (D) As (A) but with $t_{\pi/2} = 104$ ns and $t_{RF} = 35$ μs. The dotted lines are simulations according to the parameters in Table 1. Simulation of (D) is also decomposed into the two components that contribute to the spectrum.

The validity of this model for atoms that are at least two bond lengths removed from the Mn^{2+} ion has been established in previous works of Singel and co-workers (*27*, *28*) and Goldfarb and co-workers (*43*). For the α-phosphorus, the simulation gives evidence for a purely dipolar hfc tensor, and the point-dipole model leads to a distance of 4.9 Å with an estimated error of ± 0.1 Å. The value slightly exceeds the ones from the crystal structures of the wild-type protein from Tong et al. (4.59 Å (*4*)) and Milburn et al. (4.45 Å (*44*)) as well as of the mutant A59G from Hall et al. (4.66 Å (*45*)) and is slightly smaller than the one reported from previous ESEEM studies (5.3 Å (*27*)). For the β-phosphorus, we obtain 3.4 Å in agreement with the ESEEM data of Larsen et al. (3.3 Å (*27*)) and with the crystal structures (3.46 Å (*4*), 3.16 Å (*44*), 3.55 Å (*45*)). Similar values of ^{31}P hfcs were reported very recently with 35 GHz ENDOR spectroscopy on FoAs containing Mn^{2+} bound to a phosphate ion (*46*).

Furthermore, we have compared the ^{31}P spectra of the GDP complexes with the ^{31}P spectrum of the complex with the GTP analogue GppNHp. GppNHp binds to the metal ion via two phosphate groups, the β- and γ-phosphate (Figure 4, inset). Thus, this system represents a suited reference to examine whether the spectrum of the Ras(wt)·GDP complex might include an additional phosphate ion replacing one water ligand, as postulated above. The ^{31}P Davies ENDOR spectrum of the GppNHp complex is displayed in Figure 4A and shows small but significant differences to the spectrum of the GDP complexes (Figure 4B). First, the maximum of the powder pattern is shifted to smaller coupling. Second, the pake pattern is broadened. Since this spectrum consists of the β- and γ-phosphorus, we have assumed that the β-phosphorus in GppNHp has a similar hfc as in the GDP complexes, and we have subtracted the contribution of the β-phosphorus from spectrum (4B) normalized to 50% of the area of spectrum 4A and obtained spectrum 4C. The resulting powder pattern can be well simulated with one ^{31}P nucleus, which we assign to the γ-phosphorus of GppNHp. The obtained hyperfine tensor, $A_\perp = 3.3$ MHz, $A_{||} = 5.8$ MHz, translates into a point-dipole distance of 3.4 Å. The distance is consistent with the distance of 3.25 and 3.24 Å extracted from the crystal structures of Pai et al. (*47*) and Wittinghofer et al. (*48*), respectively.

The comparison between the ^{31}P spectra of the GppNHp and the GDP complexes shows that the hyperfine couplings are sensitive to the different electronic environment of the β- and γ-phosphorus. From this we conclude that the presence of an additional, bound phosphate ion in the Ras(wt)·GDP and not in the G12V complex should become visible in the ENDOR spectra. As we do not observe any differences within the line width in the spectra of the Ras·GDP complexes, we believe that this hypothesis can be ruled out.

^{13}C ENDOR Spectra. In all crystal structures of the GDP complex, Ser17 is directly ligated by its side chain hydroxyl group to the Mg^{2+} ion. In the structure of Schlichting et al. (*3*), Asp57 seemed additionally coordinated via the side chain carboxyl group to the metal ion, and it was proposed (*21*) that such a coordination pattern may be preserved for the wild-type protein complex in solution. To test this hypothesis, we have searched for the ENDOR resonances of strongly coupled ^{13}C nuclei, and we have recorded ^{13}C ENDOR spectra of the uniformly ^{13}C-labeled Ras(wt)·GDP complex as well as of the same complex containing selectively labeled 1,4-^{13}C aspartates. The spectra are displayed in Figure 5A,B.

The Mims ENDOR spectrum of uniformly ^{13}C-labeled Ras(wt)·GDP shows a 2 MHz broad powder pattern centered at the free Larmor frequency of ^{13}C. It can be very well simulated by a single ^{13}C tensor with $|A_\perp| = 0.19$ MHz, $|A_{||}| = 1.76$ MHz and a matrix peak about 0.6 MHz wide, which results from more distant ($r \geq 0.4$ nm) nuclei. We assign this coupling to the $^{13}C^\beta$ of Ser17 based on the knowledge of the crystal structure, and from comparison with DFT calculations (Table 1). The shape of the spectrum reveals

that the $A_\perp$ component has an opposite sign than $A_{||}$. From the $T_\perp$ component of the extracted ^{13}C dipolar tensor we have calculated a point-dipole distance of 3.1 Å, which is close to the distances of 3.49, 3.45, and 3.25 Å between the ion and the $^{13}C^\beta$ of Ser17 from X-ray data of Tong et al. (*4*), Milburn et al. (*44*), and Hall et al. (*45*), respectively. We note that the hfc to Ser17 had not been reported in any of the previous ESEEM studies, although an interaction had been detected (*29*).

In contrast to the uniformly ^{13}C labeled sample, the Mims ENDOR spectrum of the specific 1,4-^{13}C aspartate labeled Ras(wt)·GDP complex (Figure 5B) displays only a weak peak at the free ^{13}C Larmor frequency due to distant ^{13}C. If Asp57 were coordinated to the Mn^{2+} ion via an oxygen of its carboxyl group, the $^{13}C^\gamma$ of the carboxyl group should contribute to the ENDOR spectrum with a similar hyperfine coupling as the $^{13}C^\beta$ of Ser17. Thus, this observation unambiguously indicates that, in frozen solution, Asp57 is not a direct ligand of the metal ion. A similar observation was previously reported for the G12V mutant from ESEEM studies (*28*). The width of spectrum 5B corresponds to a point-dipole distance of 4.8 Å, which agrees with distances of 4.87, 4.81, and 4.67 Å to the 4-^{13}C of Asp57 from the X-ray structures of Tong et al. (*4*), Milburn et al. (*44*), and Hall et al. (*45*).

Finally, to test whether an amino acid other than Asp57 coordinates to the ion in the wild-type Ras·GDP complex and not in its G12V mutant, we have recorded ^{13}C Mims spectra of the uniformly ^{13}C-labeled Ras(G12V) complex (Figure 5C) and also of the uniformly ^{13}C-labeled Ras(wt)·GppNHp in complex with the Ras binding domain (RBD) of the effector Raf-kinase. According to our NMR data, this latter complex occurs in liquid solution in only one conformational state (*11*) and should serve as a reference for the contribution of two directly ligated amino acid, i.e., Ser17 and Thr35. The results show that the ENDOR spectrum of the G12V complex (5C) is undistinguishable from the wild-type one (5A), whereas the one from the Ras(wt)·GppNHp·Raf-RBD complex (5D) displays significant differences. Specifically, spectrum 5D contains features similar to 5A plus some additional contribution. On the basis of all known X-ray structures, this contribution is expected to arise from Thr35. To simulate the ^{13}C spectra, we have performed DFT calculations (see appendix) to estimate the size and the sign of the hfc tensor for Ser17 and Thr35. These values are reported in Table 1 in parentheses and were used as starting parameters in the spectral simulation procedure. As a result, the spectrum of the GppNHp complex could be well simulated with a superposition of two hfc tensors with $|A_{1\perp}| = 0.07$ MHz, $|A_{1||}| = 1.72$ MHz and $|A_{2\perp}| = 0.52$ MHz, $|A_{2||}| = 2.02$ MHz and a matrix peak about 0.6 MHz wide, as displayed in Figure 5D. The calculated point-dipole distances from the $T_\perp$ components of the extracted ^{13}C dipolar tensors are 3.4 and 3.3 Å, respectively. We tentatively assign the smaller tensor to Thr35 and the slightly larger one to Ser 17 based on the X-ray data of GppNHp and the predictions from the DFT data (see Table 1), being aware that the very small differences between the Mn^{2+}-Thr35 and Mn^{2+}-Ser17 distances observed in the X-ray structures might not be conserved in the frozen solution state. We also note that previous ESEEM data had reported a much weaker coupling to Thr35 using a different GTP analogous GppNHp and no complexation with the effector Raf-kinase (*29*). Finally, the comparison between the spectra of GppNHp and the GDP complexes strongly suggests that the spectra 5A and 5C are both contributed by only one amino acid ligand, i.e., Ser17.

To confirm this result, the relative ^{13}C ENDOR intensities (normalized to the echo intensity) of the three complexes were compared under the same experimental conditions. It is expected that the ENDOR effect measured at the same spectral position in 5A, 5C, and 5D, i.e., the edge of the powder pattern in 5A, should differ by about a factor of 2 between the GDP and the GppNHp complexes. For three different consecutive loadings of the sample, we have measured a reproducible ENDOR effect of $0.28 \pm 10\%$ for both Ras·GDP complexes and of $0.5 \pm 20\%$ for the Ras(wt)·GppNHp-effector complex. The observation strongly supports the above-mentioned result that in the GDP complexes only one amino acid, Ser17, is directly coordinated to the metal ion.

SUMMARY AND CONCLUSIONS

We have shown earlier by ^{31}P NMR spectroscopy that, in liquid solution, Ras(G12V)·Mn^{2+}·GDP exists predominantly in structural state 1 and that Ras(wt)·Mn^{2+}·GDP has an admixture of a second conformational state 2 (*21*). Simulation of the high-field EPR spectra in the presence of $H_2{}^{17}O$ with a simple model that allowed only integer values for the number of water molecules coordinated with the metal ion, had resulted in three and four water molecules coordinated to the metal ion in Ras(wt)·Mn^{2+}·GDP and Ras(G12V)·Mn^{2+}·GDP, respectively. It was plausible to correlate the EPR information with the NMR information and assign a 4-fold water coordination to state 1 and a 3-fold coordination to state 2. Since state 1 corresponded to a 6-fold coordination of the metal ion, and between state 1 and 2 no differences in the ^{55}Mn hyperfine splitting were established, i.e., the number of ligands is conserved (*49*), in state 2 an additional non-water ligand has to exist.

In the present study, we have used high-frequency 94 GHz ENDOR spectroscopy in conjunction with selective isotope labeling to search for the ligand that replaces the water molecule in the observed state 2 in solution. We have postulated that two types of ligands would be the most likely candidates: an amino acid from the protein environment or a phosphate group that is not covalently bound in the active site. All measurements were carried out at very low temperatures (4 K) after quenching the protein solutions in liquid nitrogen. We were able to detect the resonances of the strongly coupled ^{17}O, ^{31}P, and ^{13}C nuclei in the first ligation sphere of the metal ion. Quantitative analysis of the spectra leads to the hyperfine tensors and point-dipole distances summarized in Table 1.

The structural data are overall in good agreement with the published crystal structures (*4*, *44*, *45*, *47*, *48*). The ^{31}P and ^{13}C ENDOR spectra of the Ras(wt)·GDP complex and its oncogenic mutant Ras(G12V) in frozen solution do not show differences within the signal-to-noise and the ENDOR line width. Additional comparison with spectra of the GTP analogue GppNHp does not give evidence that any of the proposed candidates is ligated to the Ras(wt)·GDP complex.

Furthermore, a direct correlation with the ^{31}P NMR data using fractional states to account for different populations

of conformers was also elusive. Although these numbers likely vary with the temperature and also with the different ion, we have estimated that we should be able to observe a second conformer with a population as low as 1/3 (corresponding to the equilibrium constant $K_{12} = 0.3$ reported for the wt-GDP complex (*21*)) if the hfc values between the two conformers would differ by at least 15−20%. This estimate is based on the spectral resolution demonstrated by the comparison with the GppNHp spectra and given the signal-to-noise ratio of the spectra in the GDP complexes. We also expect that changes in the hfcs should be well observable (and not only buried in the broad powder pattern) as soon as the geometry of the coordination sphere is affected by the presence of an additional ligand that replaces one water molecule as strongly indicated by the comparison with the spectra of the GppNHp complex.

In conclusion, our results do not detect a difference in the coordination environment of the Mn^{2+} ion in the Ras(wt) and Ras(G12V) complexes, suggesting that the second conformational state observed in liquid solution, if associated with a different ligand sphere of the Mn^{2+} ion, is not populated in the frozen state.

ACKNOWLEDGMENT

We thank Prof. P. Dinse (Darmstadt) for giving us the possibility to use his W-band EPR and ENDOR spectrometer in Darmstadt. We gratefully acknowledge support by the Frankfurt Center for Scientific Computing.

APPENDIX

Quantum chemical calculations were performed using unrestricted Kohn−Sham density functional theory (DFT) methods as implemented in Gaussian 03 [*Gaussian 03*, Revision B.03, Frisch, M. J. et al. (2004); Gaussian, Inc., Wallingford, CT] and Q-Chem 2.0 [*Q-Chem 2.0*, Kong, J. et al. (2000) *J. Comput. Chem. 21*, 1532−1548]. The structural models for the Mn^{2+} binding sites were generated using relevant parts of the crystal structures of ref 4 (PDB entry 1Q21) and of ref 48 (PDB entry 5P21), for the GDP- and GppNHp complexes, respectively, and replacing Mg by Mn as well as adding all necessary H atoms. The models consist of the Mn^{2+} ion, the directly bound water molecules, the di- or triphosphate chain of the GDP or GTP(GNP), the Ser17 residue and in the case of the GppNHp complexes also the directly ligated Thr35 residue. For these structures, partial optimizations of the H atom positions were performed with Q-Chem employing the BP86 functional together with the 3-21G(d) basis set for all atoms. For the computation of the hyperfine coupling tensors with Gaussian 03, the B3PW91 hybrid functional was chosen. A 9s7p4d basis set specially developed for the calculation of ^{55}Mn hyperfine couplings [Munzarová, M., and Kaupp, M. (1999) *J. Phys. Chem. A 103*, 9966−9983] was used for Mn and the IGLO-II basis sets [Kutzelnigg, W. et al. (1991) in *NMR* − Basic Principles and Progress (Diehl, P. et al., Eds., Vol. 23, Springer Verlag, Berlin, Germany] were used for all other atoms.

REFERENCES

1. Wittinghofer, A., and Waldmann, H. (2000) Ras: a molecular switch involved in tumor formation, *Angew. Chem., Int. Ed. 39*, 4192−4214.
2. Barbacid, M. (1987) Ras Genes, *Annu. Rev. Biochem. 56*, 779−827.
3. Schlichting, I., Almo, S. C., Rapp, G., Wilson, K., Petratos, K., Lentfer, A., Wittinghofer, A., Kabsch, W., Pai, E. F., Petsko, G., and Goody, R. S. (1990) Time-resolved X-ray crystallographic study of the conformational change in Ha-Ras p21 protein on GTP hydrolysis, *Nature 345*, 309−315.
4. Tong, L., deVos, A. M., Milburn, M. V., Brunger, A., and Kim, S.-H. (1991) Crystal structures at 2.2 Å resolution of the catalytic domains of normal ras protein and an oncogenic mutant complexed with GDP, *J. Mol. Biol. 217*, 503−516.
5. Wei, Y., Zhang, Y., Derewenda, U., Liu, X., Minor, W., Nakamoto, R. K., and Somlyo, A. V. (1997) Crystal structure of RhoA-GDP and its functional implications, *Nat. Struct. Biol. 4*, 699−703.
6. Prive, G. G., Milburn, M. V., Tong, L., deVos, A. M., Yamaizumi, Z., Nishimura, S., and Kim, S.-H. (1992) X-ray crystal structures of transforming p21 ras mutants suggest a transition-state stabilization mechanism for GTP hydrolysis, *Proc. Natl. Acad. Sci. U.S.A. 89*, 3649−3653.
7. Krengel, U., Schlichting, I., Scherer, A., Schumann, R., Frech, M., John, J., Kabsch, W., Pai, E. F., and Wittinghofer, A. (1990) Three-dimensional structures of H-ras p21 mutants: molecular basis for their inability to function as signal switch molecules, *Cell 62*, 539−548.
8. Franken, S. M., Scheidig, A. J., Krengel, U., Rensland, H., Lautwein, A., Geyer, M., Scheffzek, K., Goody, R. S., Kalbitzer, H. R., Pai, E. F., and Wittinghofer, A. (1993) Three-dimensional structures and properties of a transforming and a nontransforming glycine-12 mutant of p21H-ras, *Biochemistry 32*, 8411−8420.
9. Ito, Y., Yamasaki, K., Iwahara, J., Tereda, T., Kamiya, A., Shirouzu, M., Muto, Y., Kawai, G., Yokoyama, S., Laue, E. D., Wälchi, M., Shibata, T., Nishimura, S., and Miyazawa, T. (1997) Regional polysterism in the GTP-bound form of the human c-Ha-ras protein, *Biochemistry 36*, 9109−9119.
10. Hu, J. S., and Redfield, A. G. (1997) Conformational and dynamic differences between N-ras p21 bound to GTPγS and to GMPPNP as studied by NMR, *Biochemistry 36*, 5045−5052.
11. Spörner, M., Herrmann, C., Vetter, I. R., Kalbitzer, H. R., Wittinghofer, A. (2001) Dynamic properties of the Ras switch I region and its importance for binding to effectors, *Proc. Natl. Acad. Sci. U.S.A. 98*, 4944−4949.
12. Stumber, M., Geyer, M., Kalbitzer, H. R., Scheffzek, K., and Haeberlen, U. (2002) Multiple conformational states in crystaline Ras protein in slow dynamic exchange observed by ^{31}P solid-state NMR spectroscopy, *J. Mol. Biol. 323*, 899−907.
13. Geyer, M., Schweins, T., Herrmann, C., Prisner, T. F., Wittinghofer, A., and Kalbitzer, H. R. (1996) Conformational transitions in p21ras and in its complexes with the effector protein Raf-RBD and the GTPase activating protein GAP, *Biochemistry 35*, 10308−10320.
14. Cheng, H., Sukal, S., Deng, H., Leyh, T. S., and Callender, R. (2001) Vibrational structure of GDP and GTP bound to RAS: an isotope-edited FTIR study, *Biochemistry 40*, 4035−4043.
15. Allin, C., and Gerwert, K. (2001) Ras catalyzes GTP hydrolysis by shifting negative charges from γ- to β-phosphate as revealed by time-resolved FTIR difference spectroscopy, *Biochemistry 40*, 3037−3046.
16. Allin, C., Ahmadian, M. R., Wittinghofer, A., and Gerwert, K. (2001) Monitoring the GAP catalyzed H−Ras GTPase reaction at atomic resolution in real time, *Proc. Natl. Acad. Sci. U.S.A. 98*, 7754−7759.
17. Wang, J. H., Xiao, D. G., Deng, H., Webb, M. R., and Callender, R. (1998) Raman difference studies of GDP and GTP binding to c-Harvey ras, *Biochemistry 37*, 11106−11116.
18. Futatsugi, N., and Tsuda, M. (2001) Molecular dynamics simulations of Gly-12Val mutant of p21ras: dynamic inhibition mechanism, *Biophys. J. 81*, 3483−3488.
19. Ma, J., and Karplus, M. (1997) Molecular switch in signal transduction: Reaction paths of the conformational changes in rasp21, *Proc. Natl. Acad. Sci. U.S.A. 94*, 11905−11910.
20. Glennon, T. M., Villa, J., and Warshel, A. (2000) How does GAP catalyze the GTPase reaction of Ras?: A computer simulation study, *Biochemistry 39*, 9641−9651.
21. Rohrer, M., Prisner, T. F., Brügmann, O., Käss, H., Spörner, M., Wittinghofer, A., and Kalbitzer, H. R. (2001) Structure of the metal-water complex in Ras·GDP studied by high-field EPR spectroscopy and ^{31}P NMR spectroscopy, *Biochemistry 40*, 1884−1889.

22. Spörner, M., Nuehs, A., Ganser, P., Herrmann, C., Wittinghofer, A., and Kalbitzer, H. R. (2005) Conformational states of Ras complexed with the GTP-analogs GppNHp or GppCH2p, implications for the interaction with effector proteins, *Biochemistry 44*, 2225−2236.
23. Spörner, M., Wittinghofer, A., and Kalbitzer, H. R. (2004) Perturbation of the conformational equilibria of Ras by selective mutations studied by ^{31}P NMR spectroscopy, *FEBS Lett. 578*, 305−310.
24. Bellew, B., Halkides, C. J., Gerfen, G. J., Griffin, R. G., and Singel, D. J. (1996) High frequency (139.5 GHz) electron paramagnetic resonance characterization of Mn(II)-$H_2{}^{17}O$ interactions in GDP and GTP forms of p21 ras, *Biochemistry 35*, 12186−12193.
25. Latwesen, D. G., Poe, M., Leigh, J. S., and Reed, G. H. (1992) Electron paramagnetic resonance studies of a ras p21-MnIIGDP complex in solution, *Biochemistry 31*, 4946−4950.
26. Schweins, T., Scheffzek, K., Assheuer, R., and Wittinghofer, A. (1997) The role of the metal ion in the p21 ras catalysed GTP-hydrolysis: Mn^{2+} versus Mg^{2+}, *J. Mol. Biol. 266*, 847−856.
27. Larsen, R. G., Halkides, C. J., Redfield, A. G., and Singel, D. J. (1992) Electron spin−echo envelope modulation spectroscopy of Mn^{2+}·GDP complexes of N-ras p21 with selective nitrogen-15 labeling, *J. Am. Chem. Soc. 114*, 9608−9611.
28. Halkides, C. J., Farrar, C. T., Larsen, R. G., Redfield, A. G., and Singel, D. J. (1994) Characterization of the active site of p21 ras by electron spin−echo envelope modulation spectroscopy with selective labeling: Comparisons between GDP and GTP forms, *Biochemistry 33*, 4019−4035.
29. Halkides, C. J., Farrar, C. T., Redfield, A. G., and Singel, D. J. (1996) The active site of p21 ras: conformational changes induced by the binding of nucleotides, in *Biological Structure and Dynamics* (Sarma, R. H., Sarma, M. H., Eds.) pp 249−255, Adenine Press, Schenectady, NY.
30. Arieli, D., and Goldfarb, D. (2004) Spin distribution and the location of protons in parmagnetic proteins, *Annu. Rev. Biophys. Biomol. Struct. 33*, 441−468.
31. Bennati, M., and Prisner, T. F. (2005) New developments in HF-EPR with application in structural biology, *Rep. Prog. Phys. 68*, 411−448.
32. Tucker, J., Sczakiel, G., Feuerstein, J., John, J., Goody, R. S., and Wittinghofer, A. (1986) Expression of p21 proteins in *Escherichia coli* and stereochemistry of the nucleotide-binding site, *EMBO J. 5*, 1351−1358.
33. John, J., Sohmen, R., Feuerstein, J., Linke, R., Wittinghofer, A., and Goody, R. S. (1990) Kinetics of interaction of nucleotides with nucleotide-free H-ras p21, *Biochemistry 29*, 6058−6065.
34. Herrmann, C., Martin, G. A., and Wittinghofer, A. (1995) Quantitative analysis of the complex between p21ras and the Ras-binding domain of the human Raf-1 protein kinase, *J. Biol. Chem. 2707*, 2901−2905.
35. Davis, J., Thompson, D., and Beckler, G. S. (1996) Large scale dialysis reaction using *E. coli* S30 extract systems, *Promega Notes Magn. 56*, 14−18.
36. Zawadzki, V. and Gross, H. J. (1991) Kinetics of interaction of nucleotides with nucleotide-free H-ras p21, *Nucleic Acids Res. 19*, 1948.
37. Pratt, J. M. (1984) Coupled transcription translation in prokaryotic cell-free systems, in *Transcription and Translation. A Practical Approach* (Hames, B. D., Higgins, S. J., Eds.) pp 179−209, IRL Press, Oxford.
38. Kiwaga, T., Muto, Y. and Yokoyama, S. (1995) Cell-free synthesis and amino acid- selective stable isotope labelling of proteins for NMR analysis, *J. Biomol. NMR 6*, 129−134.
39. Bennati, M., Farrar, C. T., Bryant, J. A., Inati, S. J., Weis, V., Gerfen, G. J., Riggs-Gelasco, P., Stubbe, J., and Griffin, R. G. (1999) Pulsed electron nuclear double resonance (ENDOR) at 140 GHz, *J. Magn. Reson. 138*, 232−243.
40. Raitsimring, A. M., Astashkin, A. V., Baute, D., Goldfarb, D., and Caravan, P. (2004) W-Band ^{17}O Pulsed electron nuclear double resonance study of gadolinium complexes with water, *J. Phys. Chem. 108*, 7318−7323.
41. Tan, X., Bernardo, M., Thomann, H., and Scholes, C. P. (1994) ^{17}O Hyperfine and quadrupole interactions for water ligands in frozen solutions of high spin Mn^{2+}, *J. Chem. Phys. 102*, 2675−2690.
42. Manikandan, P., Carmieli, R., Shane, T., Kalb, A. J., and Goldfarb, D. (2000) W-Band ENDOR investigation of the manganese-binding site of concanavalin A: determination of proton hyperfine couplings and their signs, *J. Am. Chem. Soc. 122*, 3488−3494.
43. Carmieli, R., Manikandan, P., Kalb, A. J., and Goldfarb, D. (2001) Proton position in the Mn^{2+} binding site of concanavalin A as determined by single-crystal high-field ENDOR spectroscopy, *J. Am. Chem. Soc. 123*, 8378−8386.
44. Milburn, M. V., Tong, L., deVos, A. M., Brunger, A., Yamaizumi, Z., Nishimura, S., and Kim, S.-H. (1990) Molecular switch for signal transduction: Structural differences between active and inactive forms of protooncogenic ras proteins, *Science 247*, 939−945.
45. Hall, B. E., Bar-Sagi, D., and Nassar, N. (2002) The structural basis for the transition from Ras-GTP to Ras-GDP, *Proc. Natl. Acad. Sci. U.S.A. 99*, 12138−12142.
46. Walsby, C. J., Telser, J., Rigsby, R. E., Armstrong, R. N., and Hoffman, B. M. (2005) Enzyme control of small-molecule coordination in FosA as revealed by ^{31}P ENDOR and ESE-EPR, *J. Am. Chem. Soc. 127*, 8310−8319.
47. Pai, E. F., Krengel, U., Goody, R. S., Kabsch, W., and Wittinghofer, A. (1990) Refined crystal structure of the triphosphate conformation of H-ras p21 at 1.35 Å resolution: Implications for the mechanism of GTP hydrolysis, *EMBO J. 9*, 2351−2359.
48. Wittinghofer, F., Krengel, U., John, J., Kabsch, W., and Pai, E. F. (1991) Three-dimensional structure of p21 in the active conformation and analysis of an oncogenic mutant. *Environ. Health Perspect.* 93, 11−15.
49. Reed, G. H., and Markham, G. D. (1984) EPR of Mn(II) complexes with enzymes and other proteins, *Biol. Magn. Res. 6*, 73−142.

BI051156K